

Learning in Deep Neural Networks Using a Biologically Inspired Optimizer

Giorgia Dellaferrera,^{1,2,*} Stanisław Woźniak,¹ Giacomo Indiveri,² Angeliki Pantazi,¹ and Evangelos Eleftheriou¹

¹*IBM Research - Zurich, Rüschlikon, Switzerland*

²*Institute of Neuroinformatics, University of Zurich and ETH Zurich, Switzerland*

(Dated: April 26, 2021)

Plasticity circuits in the brain are known to be influenced by the distribution of the synaptic weights through the mechanisms of synaptic integration and local regulation of synaptic strength. However, the complex interplay of stimulation-dependent plasticity with local learning signals is disregarded by most of the artificial neural network training algorithms devised so far. Here, we propose a novel biologically inspired optimizer for artificial (ANNs) and spiking neural networks (SNNs) that incorporates key principles of synaptic integration observed in dendrites of cortical neurons: GRAPES (Group Responsibility for Adjusting the Propagation of Error Signals). GRAPES implements a weight-distribution dependent modulation of the error signal at each node of the neural network. We show that this biologically inspired mechanism leads to a systematic improvement of the convergence rate of the network, and substantially improves classification accuracy of ANNs and SNNs with both feedforward and recurrent architectures. Furthermore, we demonstrate that GRAPES supports performance scalability for models of increasing complexity and mitigates catastrophic forgetting by enabling networks to generalize to unseen tasks based on previously acquired knowledge. The local characteristics of GRAPES minimize the required memory resources, making it optimally suited for dedicated hardware implementations. Overall, our work indicates that reconciling neurophysiology insights with machine intelligence is key to boosting the performance of neural networks.

INTRODUCTION

Artificial neural networks (ANNs) were first proposed in the 1940s as simplified computational models of the neural circuits of the mammalian brain [1]. With the advances in computing power [2], ANNs drifted away from the neurobiological systems they were initially inspired from, and reoriented towards the development of computational techniques currently employed in a wide spectrum of applications. Among the variety of techniques proposed to train multi-layer neural networks, the backpropagation (BP) algorithm [3, 4] has proven to lead to an effective training scheme. Despite the impressive progress of machine intelligence, the gap between the potential of ANNs and the computational power of the brain remains to be narrowed. Fundamental issues of ANNs, such as long training time, catastrophic forgetting [5], and inability to exploit increasing network complexity [6], need to be dealt with not only to approach the human brain capabilities, but also to improve the performance of daily used devices. For instance, reducing the training time of online learning in robotic applications is crucial to ensure a fast adaptation of the robotic agent to new contexts [7] and to reduce the energy costs associated with training.

The limitations of ANNs with respect to the brain can be largely ascribed to the substantial simplification of their structure and dynamics compared to the mammals' neural circuits. Several mechanisms of paramount importance for brain functioning, including synaptic integration and local regulation of weight strength, are typically

not modeled in BP-based training of ANNs. Some training strategies more biologically plausible than BP [8], such as the feedback alignment (FA) algorithm [9] and its direct and indirect feedback alignment (DFA, IFA) variants [10], have been proposed, yet they do not explicitly account for the neural mechanisms mentioned above. Overcoming this limitation could be key in bringing artificial networks' performance closer to animal intelligence [11].

Here, we make progress in reconciling neurophysiological insights with machine intelligence by proposing a biologically inspired optimizer that incorporates synaptic integration principles from biology, including heterosynaptic competition [12] and synaptic scaling [13]. Our approach achieves significant benefits in the training of fully connected neural networks (FCNNs), leading to a systematically faster training convergence, higher inference accuracy, better scalability of performance with network complexity, and mitigation of catastrophic forgetting. Our novel approach effectively boosts also the performance of spiking neural networks (SNNs)[14] on temporal data. These results validate the hypothesis that biologically inspired ANN and SNN models feature superior performance in software simulations [15], and provide guidelines for designing a new generation of neuro-morphic computing technologies [16].

RESULTS

Principles of biological computation. Synaptic integration is the process by which neurons combine the spike trains received by thousands of presynaptic neurons prior to the generation of action potentials [17]. Experimen-

* Electronic address: gde@zurich.ibm.com

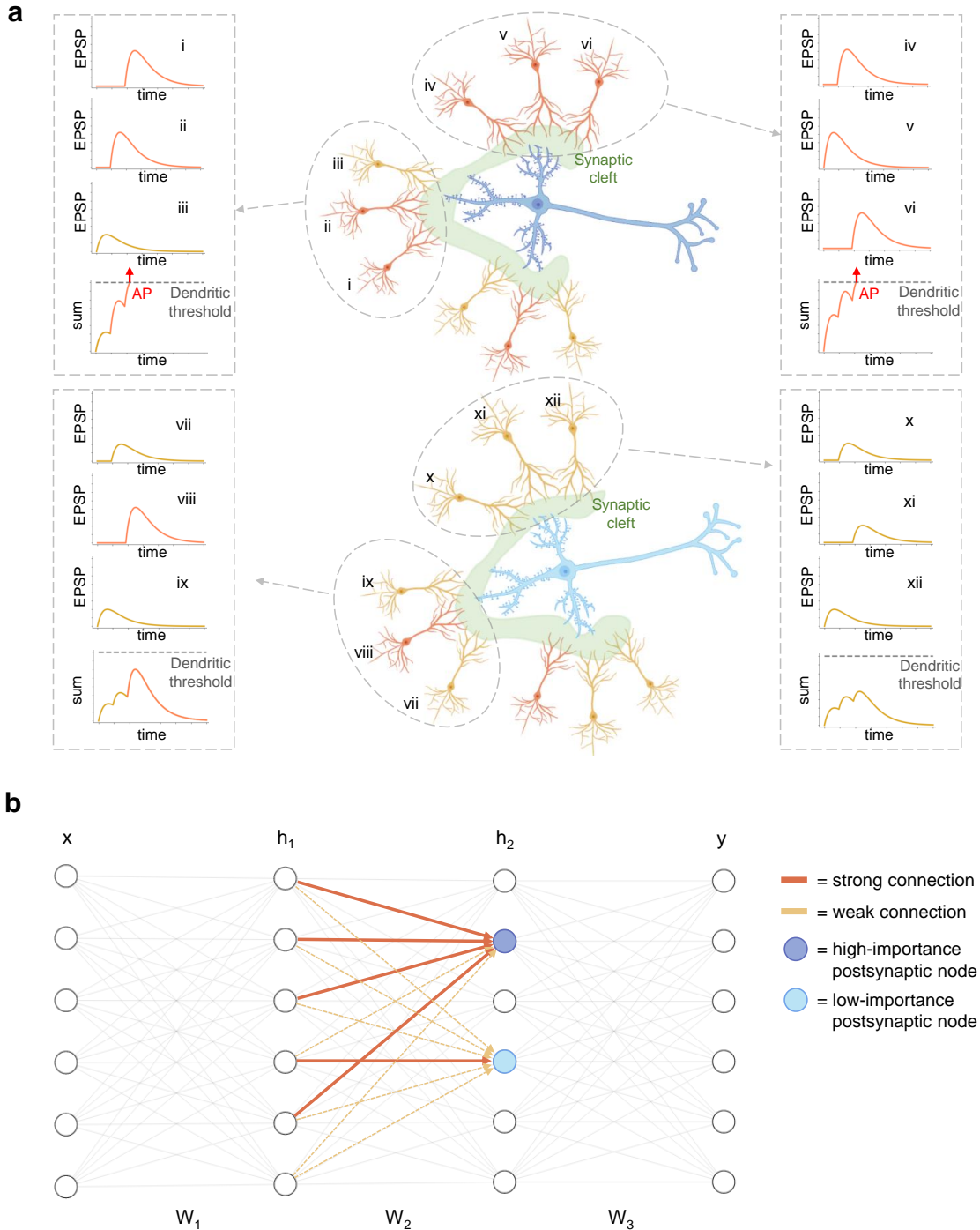


FIG. 1: (a) In biological synapses, during the process of synaptic integration, dendritic spikes can enhance the impact of synchronous inputs from dendrites belonging to the same tree. Excitatory postsynaptic potentials (EPSPs) with the same amplitude but different locations in dendritic tree may lead to different responses. For example, dendrites i , iv and $viii$ send similar signals, but only the i and iv contribute in driving an AP, since their respective trees receive sufficient further excitation from other connected dendrites. In the top image, the postsynaptic neuron (dark blue) receives inputs mostly from dendrites generating strong EPSPs (orange) and only few generating weak EPSPs (yellow). The bottom postsynaptic neuron (light blue) receives most inputs from weak-EPSPs dendrites. Because of such dendritic distribution, the dark blue neuron exhibits higher firing probability and thus its *importance* is higher with respect to the light blue neuron. (b) The structure of an FCNN is much simpler than that of biological neurons with presynaptic connections arranged in dendritic trees. However, analogously to panel (a), the *node importance* of each node arises from the distribution of the weight strength within each layer. The blue node has a high *node importance* since most of its incoming synapses are strong. Conversely, the light blue node *importance* is lower, since the presynaptic population exhibits a weaker mean strength.

tal evidence has shown that, at least in CA1 cells, input signals reaching the same postsynaptic cell from different presynaptic neurons may interact with non-linear dynamics, due to the active properties of the dendrites [18, 19]. The powerful computational abilities of neurons are suggested to stem from this complex nonlinear dynamics [20]. Figure 1(a) illustrates such a mechanism and shows how the impact, or *importance*, of each presynaptic neuron depends also on the signals delivered to the same postsynaptic neuron through other presynaptic connections. Thus, the local weight distribution can be responsible of boosting the input signal at specific nodes. Similarly to neurons in the brain, nodes in ANNs receive inputs from many cells and produce a single output. However, during training of ANNs, a mechanism taking into account the weight distribution is lacking.

Furthermore, synaptic plasticity in the brain is driven mainly by local signals, such as the activity of neighboring neurons [8]. The local interaction between synapses plays a crucial role in regulating weight changes during learning. In this context, the mechanism of heterosynaptic competition allows regulating synapse growth by limiting the total strength of synapses connected to the same pre- or postsynaptic neuron [21]. This phenomenon occurs as a nonlinear competition across synapses at each neuron. Specifically, as the summed weight of synapses into (or out of) a neuron hits a threshold, all the incoming (or outgoing) synapses to that neuron undergo a slight heterosynaptic long-term depression (“summed-weight limit rule”) [22]. Additionally, in the cortex, each neuron tends to target a specific firing rate, and synaptic strengths are regulated to keep such rates constant, despite input perturbation [13]. Synaptic scaling acts as a global negative feedback control of synaptic strength, regulating the weight changes based on the neural local activities [23–25]. These homeostatic mechanisms are typically not modeled in the training of standard ANNs, which rely on global signals instead of local information [26, 27]. Both the BP and the FA algorithms rely on the simplified training strategy of assigning the error on a weight-by-weight fashion. Each synaptic weight is updated based on its *individual* contribution to the *global* output error of the network as a response to a specific input sample. We refer to this input-specific contribution as *input-driven responsibility*. Although earlier works have attempted to encode metaplasticity (*i.e.*, the alteration of synaptic plasticity [28]) in the training of networks via weight-dependent learning rules ([29–32]), they invariably depend on a modulation of the Hebbian learning rule rather than ANNs training and do not account for the local weight distribution.

The GRAPES algorithm. The synaptic integration and the local synaptic strength regulation mechanisms are complex processes which depend on various factors, such as the large variability in size, structure, excitability, intercellular distance and temporal dynamics of synapses and dendritic spines [33]. The simple point-like structure of a synchronously operating ANN node does not allow

one to reproduce the rich dynamics enabled by the neuronal complex morphology. Hence, a direct translation of the mechanism for ANNs is not straightforward. Here, we take inspiration from the nonlinear synaptic dynamics and introduce a deep learning optimizer to boost the training of FCNNs. Our goal is to present an effective algorithm, inspired by biological mechanisms, and elucidate its potential impact on the properties of ANNs. This novel approach can also be easily applied to more biologically plausible neuronal models such as SNNs. Our algorithm builds on three observations:

- (i) In the brain, due to the spiking nature of the information, a signal is propagated only if a postsynaptic neuron receives enough input current from the presynaptic population to elicit action potentials. The stronger the input, the higher the firing rate and, thus, the amount of information propagated to the next layers.
- (ii) A single presynaptic neuron is responsible only for a fraction of the driving force that leads the postsynaptic neuron to fire. Hence, the impact of a presynaptic neuron on the downstream layers depends also on all the other presynaptic neurons connected to the same postsynaptic cell.
- (iii) If we neglect specific distributions of the inputs, the firing probability of a postsynaptic neuron depends on the average strength of the presynaptic connections. If the average strength is high, the postsynaptic neuron is more likely to reach the spiking threshold and thus to propagate further the information encoded in the presynaptic population. Therefore, the postsynaptic neuron and the related presynaptic population have a high *responsibility* on the network’s output and its potential error.

We refer to the intrinsic responsibility of the network as *network-driven responsibility*, as opposed to the *input-driven responsibility* mentioned above. Analogously, we introduce for ANNs the notion of *node importance* stemming from the node responsibility in propagating the information received from its presynaptic population to the output layer. The *node importance* is therefore related to the average strength of the synapses connected to such node. Figure 1(b) illustrates the concept of *node importance* in an FCNN. Based on this notion, we devised a novel algorithm, that we call GRAPES (Group Responsibility for Adjusting the Propagation of Error Signals). For simplicity, we begin by presenting the algorithm as a modulation of the error propagation in a network trained with BP and optimized with stochastic gradient descent (SGD). Next, we demonstrate that GRAPES can be conveniently applied also to other commonly used optimizers, such as Nesterov Accelerated Gradient (NAG) [34] and RMSprop [35], to other more biologically realistic training schemes, such as FA and DFA, and to networks with the biologically realistic dynamics of spiking neurons.

The GRAPES algorithm modulates the error signal at each synaptic weight based on two quantities: the *node*

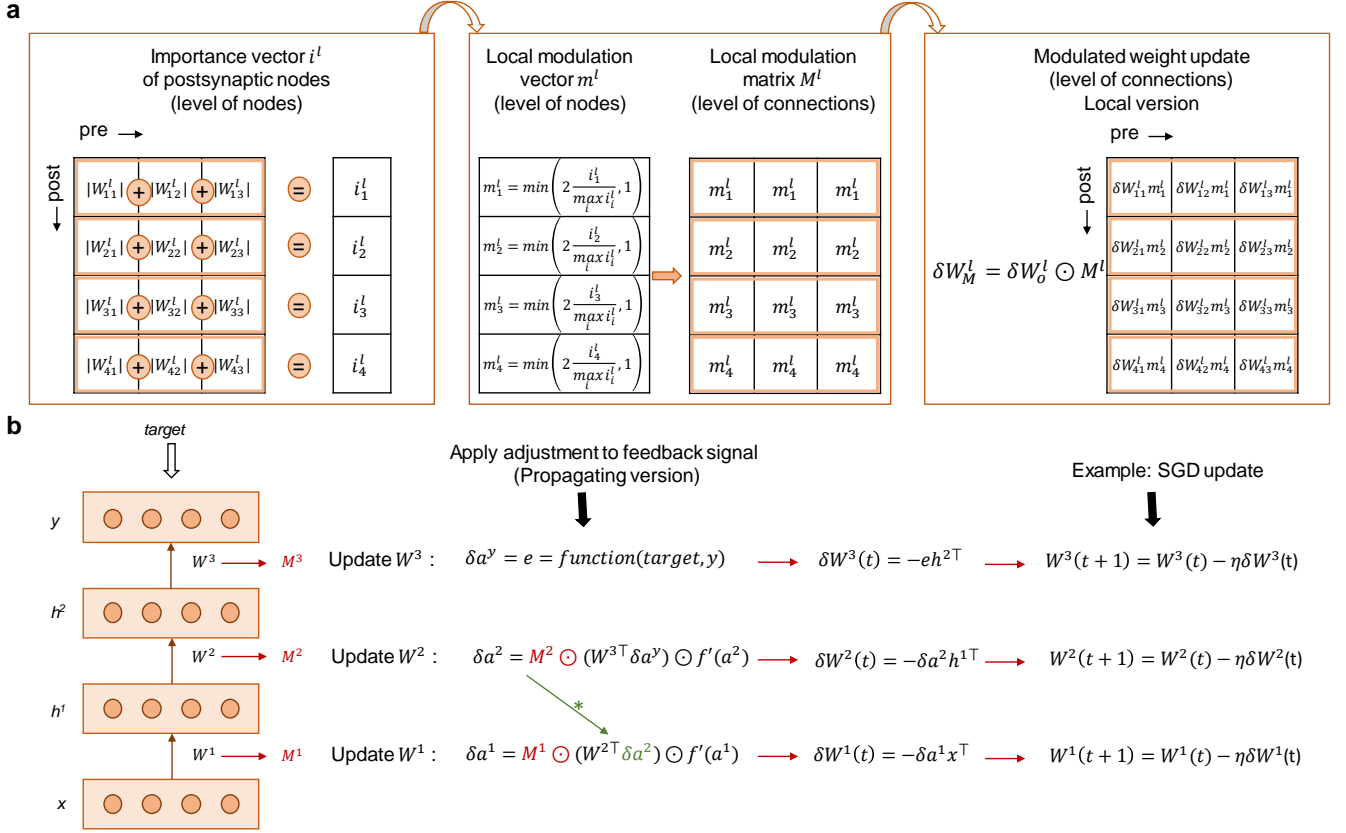


FIG. 2: **(a)** The computation of the importance vector for one hidden layer, based on the associated weight matrix, is followed by the computation of the local modulation vector, based on the node importance. In the local version, GRAPES adjusts the weight update through the Hadamard multiplication of the initial weight-update matrix with the local modulating vector. **(b)** Algorithm for the propagation of the modulation factor to the upstream layers in a two-hidden layer network. The activations in the network are computed as $a^1 = W^1 x$, $h^1 = f(a^1)$ and $a^2 = W^2 h^1$, $h^2 = f(a^2)$, and the network output as $a^y = W^3 h^2$, $y = f_y(a^3)$. Note that δa^2 is adjusted through the modulation matrix M^2 and such adjustment also affects the upstream layer since δa^2 contains δa^1 .

importance and the *local modulation factor*. Mathematically, we define the *node importance* of a given node n belonging to layer l as the sum of the absolute strength over all weights of layer l whose postsynaptic neuron is n

$$i_n^l = \sum_{\text{pre}=1}^N |W_{\text{post}=n, \text{pre}}^l|, \quad (1)$$

where N is the number of incoming connections to node n . Alternatively, in specific cases discussed further in the paper, the *node importance* may also be obtained from the sum of the absolute strength of all weights of layer $l + 1$ outgoing from the same presynaptic neuron.

The *importance vector* i^l for layer l contains the *node importance* values for each postsynaptic node n in l . By normalizing the importance vector by its maximal value, multiplying it by 2 and lower-bounding by 1, we obtain the *local modulation vector*

$$m^l = \min \left(2 \frac{i^l}{\max(i^l)}, 1 \right), \quad (2)$$

whose elements are bounded in the range $1 \leq m^l \leq 2$. Such an interval has been defined on the basis of an empirical optimization. The n -th *local modulation factor* is the n -th element of the resulting vector and indicates the responsibility of the postsynaptic node n and its associated connected weights on the output of the network. In order to build the *local modulation matrix* M^l for layer l , the *local modulation vector* is tiled as many times as the presynaptic population size. Each element of the matrix is associated with one synaptic weight of layer l . Therefore, by construction, the modulation has the same value for all weights $W_{\text{post}=n, \text{pre}}^l$ connected to the same postsynaptic neuron n .

With these quantities at hand, in the local version of GRAPES, we adjust the error signal in layer l through a Hadamard multiplication of the weight-update matrix with the local modulation matrix. The weight-change matrix, in which each row corresponds to a post-synaptic node and each column to a pre-synaptic node, is modu-

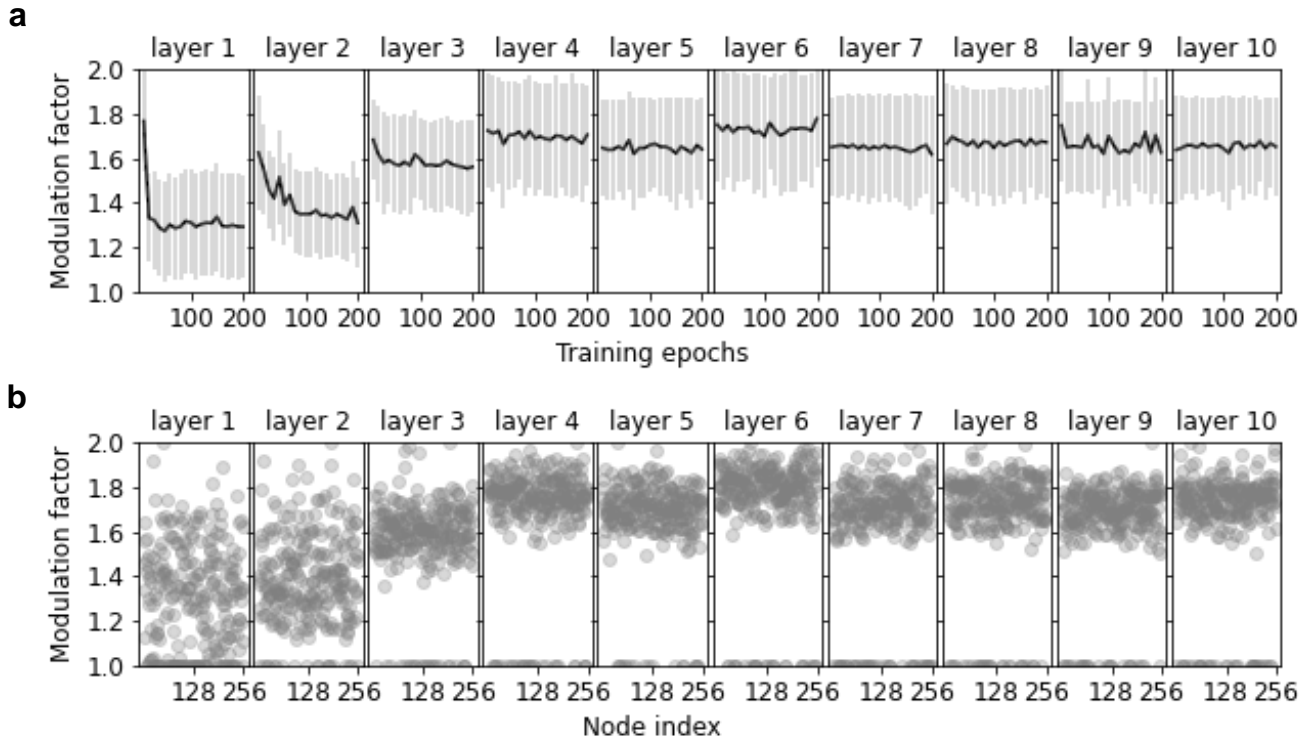


FIG. 3: (a) Mean and standard deviation dynamics of the modulation factors for a 10×256 tanh network, with 10% dropout and weight decay, trained with BP, SGD and GRAPES modulation for 200 training epochs. The modulation factors are recorded for each layer every 10 epochs. (b) Distribution of the modulation factors at the end of training.

lated row-wise:

$$\delta W_M^l = \delta W_o^l \odot M^l. \quad (3)$$

The main steps of the computation of importance vector, local modulation vector and matrix for a single hidden layer l , and the update step of the local version of GRAPES are summarized in Figure 2(a).

In the propagating version of the algorithm, the modulation factor is incorporated in the error signal of each layer and propagated to the upstream layers, where it is incorporated in the respective weight updates. In Figure 2(b) we outline the algorithm for the propagation of the modulation factor in a two-hidden layer network. The propagating version provides the greatest benefits in terms of classification accuracy and convergence speed compared to the local version, as shown in Supplementary Table S1. Hence, the propagating version of the algorithm is the default method adopted in the simulations. Finally, the weight update obtained by applying the GRAPES modulation to SGD can be expressed as:

$$W^l(t+1) = W^l(t) - \eta \delta W_M^l(t). \quad (4)$$

GRAPES does not change the computational complexity of SGD and, since the modulation factor is computed only after the parameter update (*e.g.*, at the end of each

mini-batch), the additional computations are negligible for large mini-batch size.

By construction, the error signal modulation implemented in GRAPES presents some analogies with the biological mechanisms of heterosynaptic competition and synaptic scaling. Firstly, the *node importance* is defined as the sum of the synaptic weights connected to the same node. As in heterosynaptic competition, the information on the total synaptic strength is used to modulate the weight magnitude. However, while in heterosynaptic competition the total synaptic weight is used to solely determine depression by changing directly the weights [22], in GRAPES the total weight information is used to adjust the weight update, hence leading to both strengthening or weakening of the synapses. Secondly, by definition, the *local modulation factor* in GRAPES is equal for all synapses incoming to the same node. This leads back to synaptic scaling, in which a neuron-specific multiplicative scaling factor adjusts the weights of the synapses connected to the same neuron based on the local activity so that the neuron maintains a target firing rate.

Figure 3(a) displays the evolution of the modulation factor during training of a 10 hidden layer network. The dynamics of the modulation factor are different for each layer. The mean of the modulation factor exhibits the

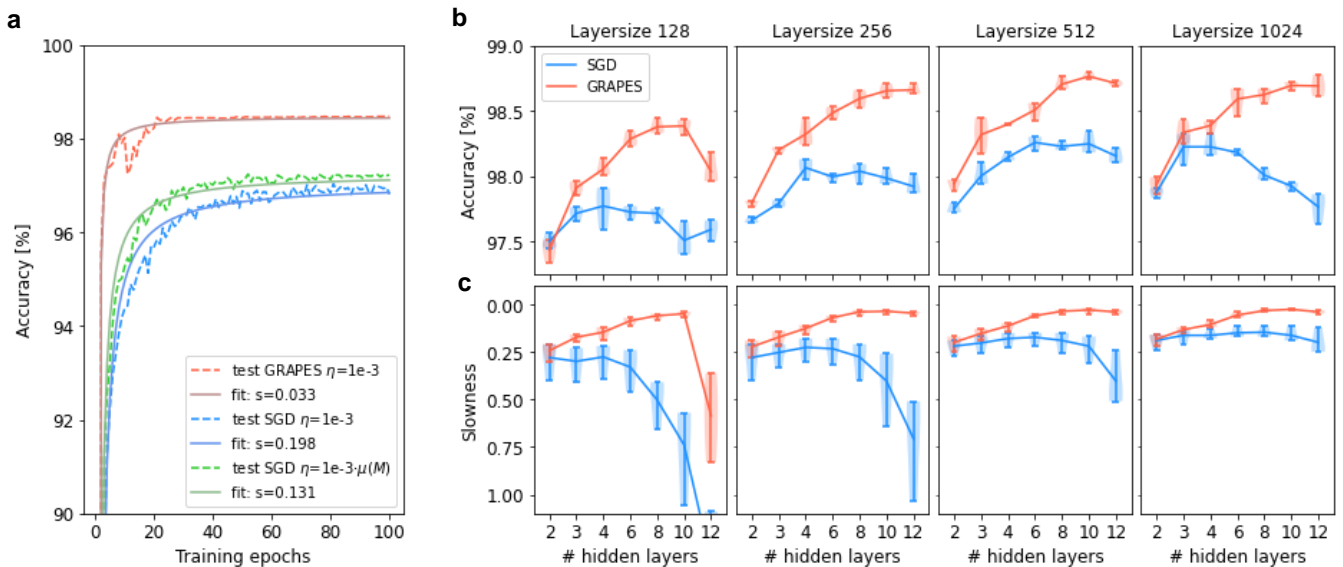


FIG. 4: (a) Testing curve (dotted line) and fit using the *plateau function* (solid line) for the 10×256 ReLU network, trained without dropout on the MNIST data set. The red curves are related to the network trained with GRAPES, whereas the green and blue curves to the networks trained with SGD with equal and increased learning rate respectively. The fit is performed on the initial 100 epochs. (b) Test accuracy of networks with different layer size as a function of the number of hidden layers. (c) Convergence rate of networks with different layer size as a function of the depth. The shaded area around the standard deviation bar shows the distribution of the results of five runs. In (b) and (c), the learning rate of SGD networks is uniformly increased. Despite the higher learning rate, the SGD networks exhibit a much worse convergence rate in comparison to GRAPES.

most pronounced decay in the first three hidden layers, whereas it either decreases very slowly or remains constant in the downstream hidden layers. In Figure 3(b), we show the distribution of the modulation factors for each layer after training. In each layer, a subset of the modulation factors is equal to 1, due to the lower bounding operation in Eq. 2. The remaining values are distributed with mean and variance specific to each layer. Therefore, based solely on the current state of the network weights, GRAPES offers a simple approach to modulate the error signal at each synapse using node-specific factors whose temporal evolution, mean and variance can be different for each hidden layer. Note that, for some layers, the decrease of the modulation factor with respect to its initial value resembles a learning rate decay scheme [36]. Compared to the classical learning-rate-schedules, GRAPES provides two main advantages. First, to apply a learning rate decay, a time-consuming search of the best decay scheme and its hyperparameters is required for each network setting and task. Instead, the spontaneous decay provided by GRAPES does not need to be optimized in advance, thus allowing the modulation factor to naturally adapt to different architectures and data sets. Furthermore, while with the conventional learning-rate-schedule approach the learning rate is equal for each parameter, GRAPES allows the update step to be adjusted differently for each weight. Specifically, we have shown in Figure 3 that GRAPES implements a dynamic learning

schedule for each weight. We demonstrate the stability of such a learning schedule by analytically proving the convergence properties of GRAPES in Supplementary Note 1.

Simulation results on handwritten digit classification. To illustrate the benefits of GRAPES on the training of ANNs, we have enhanced the standard minibatch SGD by incorporating the GRAPES modulation scheme, and are referring to it as “GRAPES”. We initially compare the performance of GRAPES against standard minibatch SGD, which from now on we will simply call “SGD”, on the MNIST data set [37].

To evaluate the convergence rate, we relied on a Michaelis Menten-like equation [38] and introduced the novel *plateau equation for learning curves*:

$$\text{accuracy} = \frac{\text{max_accuracy} \cdot \text{epochs}}{\text{slowness} + \text{epochs}}. \quad (5)$$

By fitting the test curve to this function, we can extract the *slowness* parameter, which quantifies how fast the network reduces the loss during training. Mathematically, the *slowness* value corresponds to the number of epochs necessary to reach half of the maximum accuracy. Hence, the lower the *slowness*, the faster the training. In our simulations, we perform the fit on the first 100 epochs. The graphical representation of the *plateau curve* is given in the Supplementary Figure S1.

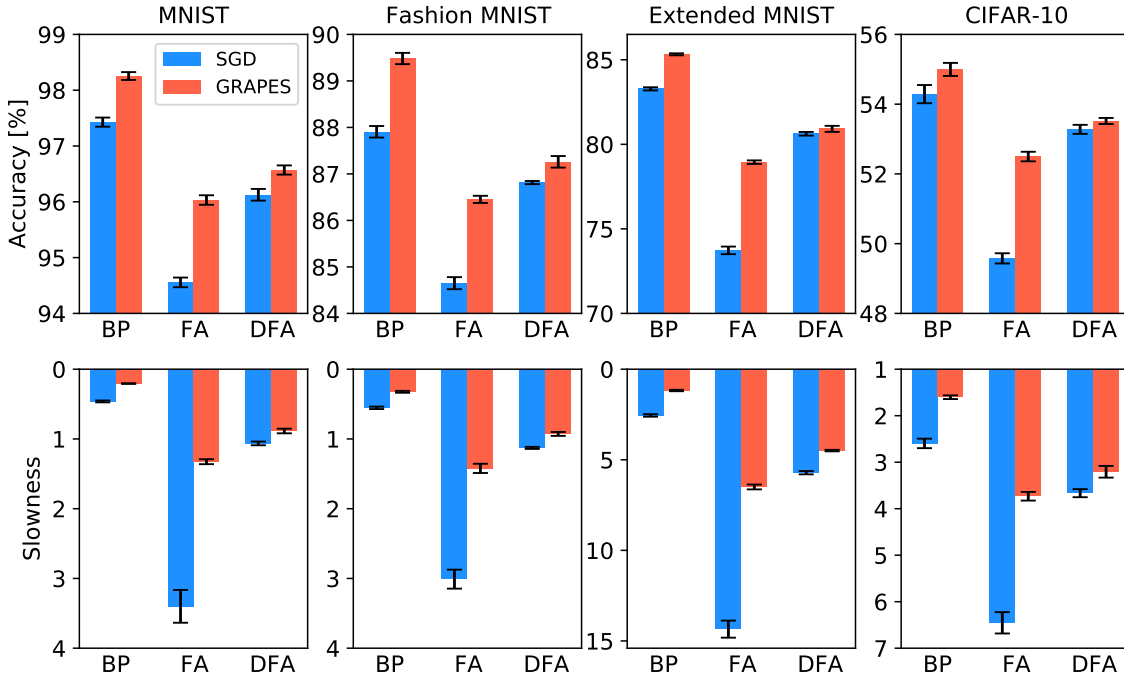


FIG. 5: Test accuracy and convergence rate in terms of slowness value for 3×256 ReLU networks, with 10% dropout, trained with BP, FA and DFA on MNIST, Fashion MNIST, Extended MNIST, and CIFAR-10 data sets. The slowness parameter is computed by fitting the initial 100 epochs.

Figure 4(a) reports test curves and related *slowness* fits for 10×256 ReLU networks, trained on the MNIST data set. The red and blue curves refer to GRAPES and SGD-based training respectively, with the same learning rate. As the average of the modulation factor is larger than one (see Figure 3), one needs to ensure that the training improvements are not solely due to a greater mean of the learning rate. Therefore, we also performed SGD-based training with a learning rate that is multiplied by the mean of the modulation factor at the beginning of training. The results of these simulations are shown as a green dashed line in Figure 4(a). The testing curve for the GRAPES model saturates at a significantly higher accuracy plateau compared with those of the SGD models. Furthermore, the test curve for GRAPES rises much earlier and in a steeper manner - leading to a consistently smaller *slowness* parameter - compared with the test curves of the networks trained with SGD, both with equal and uniformly increased learning rate. This demonstrates that the key for improving the convergence lies in the non-uniform modulation of the error signal. Supplementary Table S2 shows that GRAPES exhibits the described improvements in accuracy and convergence rate under a wide range of network configurations. On the basis of these findings, it is worth drawing the two following observations. Firstly, even in the case where GRAPES is

used with a smaller learning rate than SGD (network configuration with 10 hidden layers and tanh activations), it converges faster than SGD. Secondly, GRAPES combined with the deformation strategy in Ref. [39], reaches a test accuracy of 99.56%, which is rarely attainable by non-convolutional architectures. For additional details, see Supplementary Table S2.

Previous work in Ref. [6] empirically showed that, as the number of trainable parameters in deep neural networks increases, the network performance initially improves and then saturates. We demonstrated that GRAPES is able to mitigate such limitation of SGD by exploiting the increasing complexity of FCNNs in terms of both layer size and network depth. Figure 4(b) shows the accuracy results for models with increasing layer size and depth, and Figure 4(c) depicts the related slowness parameter. Not only GRAPES achieves higher accuracy than SGD for most models, but, importantly, the accuracy results indicate a rising trend as the network depth increases. On the other hand, with SGD the accuracy either saturates or deteriorates for increasing network complexity. In addition, GRAPES exhibits a much faster convergence compared with SGD. Unlike SGD, GRAPES benefits from a greater network complexity and converges even faster when deeper networks are used, indicating that GRAPES enhances the most relevant weight up-

dates.

Performance under various learning rules and data sets. GRAPES can be combined with a wide range of momentum-based optimizers (*e.g.*, NAG, rmsprop) and credit assignment strategies (*e.g.*, FA, DFA, IFA). When combined with DFA, the computation of the modulation factor requires a modification. Since in DFA the propagation of the error occurs directly from the output layer to each hidden layer, the dimensionality of the error terms is different with respect to BP. Therefore, in order to incorporate the modulation factor in the error term, we compute the *importance* based on the presynaptic grouping

$$i_n^l = \sum_{\text{post}=1}^K |W_{\text{post,pre}=n}^{l+1}|, \quad (6)$$

where K is the number of outgoing connections from node n in layer l .

Figure 5 shows the improvements obtained by GRAPES in terms of accuracy and convergence rate when applied to BP, FA and DFA over a range of data sets (MNIST, Fashion MNIST [40], Extended MNIST [41] and CIFAR-10 [42]). Firstly, the same improvements observed with MNIST and BP are obtained also with more complex data sets. Secondly, the performance of FA, which is the worst across all network configurations when combined with SGD, is significantly improved by GRAPES. Thus, GRAPES allows FA models to approach the performance of DFA models trained with SGD. Finally, when applied to DFA, GRAPES shows better accuracy and quicker convergence in all cases.

Supplementary Table S3 shows that comparable improvements in accuracy and slowness are obtained under a wide range of network settings. We remark that GRAPES enables the FA schemes to scale to complex settings (deeper networks, more complicated tasks such as CIFAR-10) in which they have been recognized to fail [43]. Furthermore, in Supplementary Tables S4-S7 we report the performance of GRAPES applied on several feed-forward models proposed in Ref. [10] and Ref. [44]. These results demonstrate that, when GRAPES is applied on top of momentum-based optimizers, in most cases it leads to better accuracy than such optimizers in their original formulation.

Mitigation of catastrophic forgetting. Catastrophic forgetting refers to the phenomenon affecting neural networks by which the process of learning a new task causes a sudden and dramatic degradation of the knowledge previously acquired by the system [5]. This represents a key limitation of ANNs, preventing the successful reproduction of continual learning occurring in the human brain [45, 46]. Here, we show that the application of GRAPES mitigates, to a certain extent, the effects of catastrophic forgetting in ANNs. To analyze catastrophic forgetting in a sequence of supervised learning tasks, we have adopted the protocol proposed in Ref. [47]. For each task, we randomly generate a permutation pattern of a fraction

of image pixels and we apply it to all the training and testing samples of the MNIST data set. We perform the training sequentially for all tasks for a fixed number of epochs, and, after each training epoch, we test the network performance of all the previously learnt tasks. Figure 6 compares the testing accuracy for the 3×256 network with ReLU activations trained with (a) SGD and (b) GRAPES. For each task, 600 random permutations are applied. We observe that, compared with SGD, the drop in accuracy observed after learning each new task is considerably reduced when GRAPES is applied. Furthermore, we analyzed the effect of GRAPES under a second interesting aspect of incremental learning: the generalization to unseen tasks. Following the paradigm proposed in Ref. [48], we compute the *per-task-future-accuracy*, by testing the model performance on tasks it has not been trained on yet. We initially used the same protocol with 600 permutations as in Figures 6(a) and 6(b), hence different tasks are only slightly correlated with each other (the total number of pixels is 784). Figure 6(c) shows that in most cases the networks trained with GRAPES show better generalization capability on unseen permutations. The absolute accuracy is, though, very low. Thus, we decreased the number of permutations to 300, leading the tasks to have a stronger correlation with each other. The results are reported in Figure 6(d). We observe that both SGD and GRAPES achieve well above-chance level accuracy. The generalization capability increases with the number of tasks learnt. Consistently with the results obtained with 600 permutations, GRAPES in most cases leads to higher accuracy than SGD. Therefore, both in the case of almost uncorrelated and partially correlated tasks, GRAPES proves to be more effective in achieving knowledge transfer to future tasks compared to SGD. We ascribe this remarkable result mainly to two properties of GRAPES. First, GRAPES achieves a lower training error in fewer training epochs, thereby enabling the network to learn a new task with fewer parameter updates. As a consequence, the weight distribution after learning a new task remains closer to the weight distribution learnt during the previous task. Secondly, GRAPES enhances the updates related to a subset of parameters based on their importance. At each new task, such subset may vary, thus the learning focuses on different groups of synapses, thereby better preserving knowledge on the old tasks.

Application of GRAPES to biologically inspired neural networks. SNNs are neural network models that attempt to mimic the complex neuronal dynamics of the mammalian brain [14]. Moreover, the development of SNNs is driven by the ultimate goal to implement embedded neuromorphic circuits, with high parallelism, low-power consumption, fast inference, event-driven processing, and online learning [49, 50]. Given its biological inspiration, GRAPES holds great potential to boost the performance of SNNs. We apply GRAPES on SNN architectures implemented through the spiking neural unit (SNU) approach [51], which unifies SNNs with recurrent ANNs by abstracting the dynamics of a LIF spiking neu-

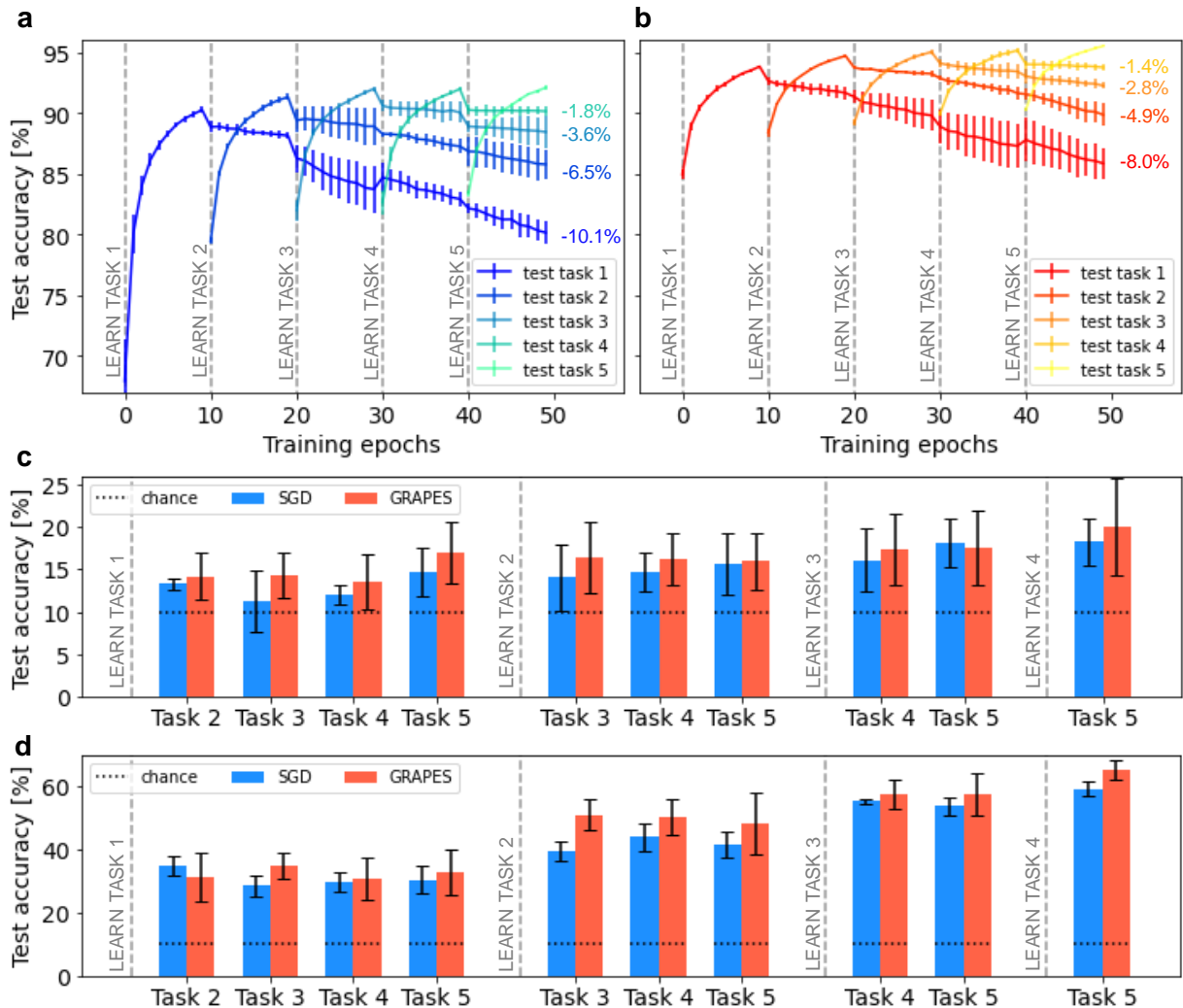


FIG. 6: Following the protocol in Ref. [47] for catastrophic forgetting, we trained 3×256 ReLU networks with (a) SGD and (b) GRAPES on a sequence of tasks. Each task is defined by a random pattern of 600 pixel permutations, which is applied to all MNIST train and test images. The networks are trained sequentially on each task for 10 epochs. At the end of each training epoch, the networks are tested on both the task they are being trained on and the tasks they have already learnt (e.g., while learning task 1 they are tested only on task 1, and while learning task 2 they are tested on both task 2 and 1 to observe performance degradation on task 1). Panels (a) and (b) show the resulting test curves. Panels (c) and (d) report the *per-task-future-accuracy* ([48]) on unseen tasks. The tasks are defined by 600 (panel c) and 300 (panel d) pixel permutations, respectively. The networks are first trained on each task for 10 epochs and then tested on all the unseen tasks (e.g., after learning task 1, the per-task-future-accuracy is reported for unseen tasks 2,3,4,5).

ron [52] into a simple recurrent ANN unit. SNUs may operate as SNNs, with a step function activation, or as more conventional RNNs, with continuous activations. The non-spiking variant is called soft SNU (sSNU).

We trained both SNU and sSNU models on temporal data derived from the MNIST data set. To that end, we encoded the MNIST handwritten digit examples into spikes using the rate coding method as described in [51]. The depth of the network for optimal performance was found to be 3 hidden layers for SNU, and

2 hidden layers for sSNU. Figure 7(a) reports the accuracy results. For both models, GRAPES surpasses the classification accuracy obtained with SGD for different layer sizes. Furthermore, GRAPES renders the networks robust against hyperparameter choice and model complexity. As can be seen in Figure 7(b) for SNUs, the convergence of SGD-based training is heavily affected by changes in the magnitude of the learning rate η . As η is decreased, the number of training epochs needed to trigger efficient learning dramatically rises. When GRAPES

DISCUSSION

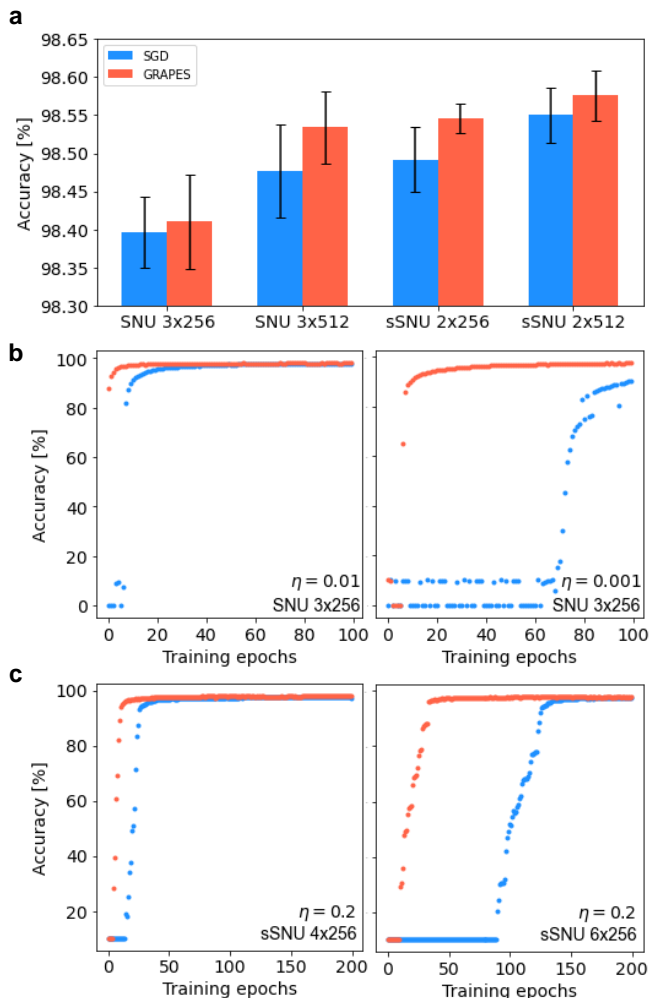


FIG. 7: (a) Test accuracy for SNU and sSNU networks with 3 and 2 hidden layers, respectively. (b) Test curves for SNU 3×256 networks with decreasing values for the learning rate η . Left hand-side: $\eta = 0.01$. Right hand-side: $\eta = 0.01s$. The initial 100 training epochs are shown. (c) Test curves for sSNU networks with increasing number of hidden layers. Left hand-side: 4×256 networks. Right hand-side: 6×256 networks. In (b) and (c) the curves correspond to a single run.

is introduced, the model reaches well above-chance performance in only a few epochs. Furthermore, as illustrated for sSNUs in Figure 7(c), SGD struggles in triggering learning of networks with increasing depth, requiring almost 100 epochs to start effective training of 6 hidden layer networks. GRAPES overcomes this issue, by enabling the deep models to converge with a lower number of epochs.

Inspired by the biological mechanism of non-linear synaptic integration and local synaptic strength regulation, we proposed GRAPES (Group Responsibility for Adjusting the Propagation of Error Signals), a novel optimizer for both ANN and SNN training. GRAPES relies on the novel concept of *node importance*, which quantifies the responsibility of each node in the network, as a function of the local weight distribution within a layer. Applied to gradient-based optimization algorithms, GRAPES provides a simple and efficient strategy to dynamically adjust the error signal at each node and to enhance the updates of the most relevant parameters. Compared with optimizers such as momentum, our approach does not need to store parameters from previous steps, avoiding additional memory penalty. This feature makes GRAPES more biologically plausible than momentum-based optimizers as neural circuits cannot retain a significant fraction of information from previous states [53].

We validated our approach with ANNs on four static data sets (MNIST, CIFAR-10, Fashion MNIST and Extended MNIST) and with SNNs on the temporal rate-coded MNIST. We successfully applied GRAPES to different training methods for supervised learning, namely BP, FA and DFA, and to different optimizers, *i.e.*, SGD, RMSprop and NAG. We demonstrated that the proposed weight-based modulation leads to higher classification accuracy and faster convergence rate both in ANNs and SNNs. Next, we showed that GRAPES addresses major limitations of ANNs, including performance saturation for increasing network complexity [6] and catastrophic forgetting [5].

We suggest that these properties stem from the fact that GRAPES effectively combines in the error signal information related to the response to the current input with information on the internal state of the network, independent of the data sample. Indeed, GRAPES enriches the synaptic updates based on the *input-driven responsibility* with a modulation relying on the *network-driven responsibility*, which indicates the potential impact that a node would have on the network's output, independently on the input. Such training strategy endows networks trained with GRAPES with the ability to achieve convergence in a lower number of epochs, as the training is not constrained to information relative to the presented training samples only. For the same reason, such networks present better generalization capability than SGD both when tested on the learnt tasks and when presented with unseen tasks in continual learning scenarios. In this context, we identify parallelism with plasticity types in the brain. The change in synaptic strength in response to neuronal activity results from the interplay of two forms of plasticity: homosynaptic and heterosynaptic. Homosynaptic plasticity occurs at synapses active during the input induction, thus is input-specific and associative, as the *input-driven responsibil-*

ity. Instead, heterosynaptic plasticity concerns synapses that are not activated by presynaptic activity and acts as an additional mechanism to stabilize the networks after homosynaptic changes [54, 55]. Therefore, similarly to the *network-driven responsibility*, heterosynaptic plasticity does not exhibit strict input specificity.

A further origin of the benefits of GRAPES stems from the adjustment of the error signal. The nonuniform distribution of the modulation factor, combined with the propagation to upstream layers, allows GRAPES to greatly enhance a subset of synaptic updates during training. Hence, small groups of synapses are enabled to strengthen or weaken to a much larger extent than with SGD. From preliminary investigation, GRAPES appears to convey the network weights toward more biologically plausible distribution, specifically heavy-tailed distributions [56–59]. Additional details are provided in Supplementary Note 2. We suggest that the properties exhibited by GRAPES could stem from such weight distribution. Ongoing work in our group is currently seeking a more comprehensive understanding of this phenomenon.

Remarkably, our results suggest that GRAPES offers a promising strategy for mitigating the performance degradation caused by hardware-related constraints, such as noise and reduced precision, as discussed in Supplementary Note 3. We highlight that these constraints reflect biological circuits in many aspects, as the synaptic transmission is affected by noise and the neural signal is quantized. Interestingly, GRAPES retains many similarities with biological processes. We, therefore, envision that the biological mechanisms underlying GRAPES may play a central role in overcoming the limitations associated with hardware-related constraints. Furthermore, we suggest that such brain-inspired features are at the origin of the benefits of GRAPES on biologically-inspired models. Indeed, we have demonstrated that GRAPES not only improves BP-based training of standard ANNs, but additionally boosts significantly the performance of networks trained with biologically plausible credit assignment strategies, such as FA and DFA, and networks relying on the dynamics of spiking neurons. Both the FA algorithms and the SNN models are crucial steps towards bridging biological plausibility and machine learning. However, at the present stage, they can only achieve a limited performance compared to ANNs trained with BP [43, 50]. For instance, as shown in the Results section, both the FA and SNNs approaches suffer from lower accuracy and convergence rate compared to BP, and SNNs training is severely affected by changes in network complexity and hyperparameters. Thanks to an efficient modulation of the error signal which enhances the updates of the most important parameters, GRAPES reduces the impact of such limitations, thereby narrowing the gap between the performance of bio-inspired algorithms and standard ANNs.

To conclude, our findings indicate that incorporating GRAPES and, more generally, brain-inspired local factors in the optimization of neural networks paves the

way for pivotal progress in the performance of biologically inspired learning algorithms and in the design of novel neuromorphic computing technologies.

METHODS

MNIST data set. We train FCNNs with 3 and 10 hidden layers, each consisting of either 256 or 512 hidden nodes. The activation functions chosen for the hidden layers are rectified linear unit (ReLU) or hyperbolic tangent (tanh). The output activation is softmax with cross-entropy loss function. With ReLU hidden nodes the weights are initialized according to [60], with tanh units according to [61]. The minibatch size is fixed to 64. The learning rate η is optimized for the different models, separately for SGD and GRAPES, and is kept fixed during training. Supplementary Table S8 reports the optimized learning rate for all simulations. We investigate the performance both without dropout [62] and with moderate dropout rates of 10% and 25%. We also show the accuracy improvement of the models that are trained with an augmented version of the data set, built by applying both affine and elastic deformation on the training set, similarly as proposed in Ref. [39]. To compute the accuracy, we train the models on the training set and after each epoch we test the performance on the test set. Following the strategy in Ref. [39], we report the best test accuracy throughout the entire simulation. For all settings, we average the result over five independent runs.

Scalability to complex networks. We train networks with layer sizes ranging from 128 to 1024 and with depth from 2 to 12 hidden layers. Each network is trained with ReLU, 10% dropout rate and for 200 epochs. The learning rate is kept constant to $\eta = 0.001$. As in the previous section, we report the best testing accuracy obtained throughout the entire training, averaged over five runs.

Catastrophic forgetting. For each task, 600 random permutations are applied. We train 3×256 ReLU FCNN networks on the training samples using shuffling and minibatch processing for a fixed number of epochs. We set the number of training epochs per task to 10. We use a constant learning rate $\eta = 0.001$. We introduce a dropout rate of 10%. For all settings, we average the result over five independent runs.

Spiking Neural Networks. We train SNU and sSNU networks on the rate-coded MNIST data set. The dynamics of the units and the training protocol are the same as described in Ref. [51]. The only difference with respect to the original SNU network in Ref. [51] is the introduction of a soft-reset to smoothen the training process of the spiking units. We performed a grid-search for the hyperparameters. For the SNU networks the optimal configuration is 3-hidden layer and constant learning rate $\eta = 0.1$. For sSNU models the optimal configuration is 2-hidden layers with constant $\eta = 0.2$. The networks are

trained for 200 epochs. The number of steps of input presentation is set to $N_s = 20$ during train and $N_s = 300$ during test. The mean and standard deviation of the final accuracy are computed over 5 runs.

Programming. The learning experiments of the ANN simulations were run using custom-built code in Python3 with the Numpy library. The SNU and sSNU-based simulations were performed using the original TensorFlow code from the Supplementary Material of [51].

Data availability. The data sets used for the simulations are publicly available. Example program codes used for the numerical simulations are available on request.

ACKNOWLEDGMENTS

We thank T. Bohnstingl, M. Dazzi, S. Nandakumar, A. Stanojevic, M. Pizzochero and our colleagues at the IBM

Neuromorphic Computing and IO Links team for fruitful discussions. Figure 1 has been created with BioRender.com.

AUTHOR CONTRIBUTIONS

G.D. conceived the idea. All the authors identified the properties of the proposed algorithm in terms of error modulation, scalability, catastrophic forgetting and behaviour under hardware constraints. G.D. designed and performed the simulations. All authors analyzed the results. G.D. wrote the manuscript with input from the other authors.

-
- [1] McCulloch, W. S. & Pitts, W. A logical calculus of the ideas immanent in nervous activity. *The bulletin of mathematical biophysics* **5**, 115–133 (1943).
- [2] Thompson, N. C., Greenewald, K., Lee, K. & Manso, G. F. The computational limits of deep learning (2020). Preprint at <https://arxiv.org/abs/2007.05558>.
- [3] Rumelhart, D. E., Durbin, R., Golden, R. & Chauvin, Y. *Backpropagation: The Basic Theory*, 1–34 (L. Erlbaum Associates Inc., USA, 1995).
- [4] Schmidhuber, J. Deep learning in neural networks: An overview. *Neural Networks* **61**, 85–117 (2015).
- [5] French, R. M. Catastrophic forgetting in connectionist networks. *Trends in Cognitive Sciences* **3**, 128 – 135 (1999).
- [6] Ba, J. & Caruana, R. Do deep nets really need to be deep? In *Advances in Neural Information Processing Systems*, vol. 27, 2654–2662 (2014).
- [7] Polydoros, A. & Nalpantidis, L. Survey of model-based reinforcement learning: Applications on robotics. *Journal of Intelligent & Robotic Systems* **86**, 153– (2017).
- [8] Whittington, J. & Bogacz, R. Theories of error backpropagation in the brain. *Trends in Cognitive Sciences* **23**, 235–250 (2019).
- [9] Lillicrap, T. P., Cownden, D., Tweed, D. B. & Akerman, C. J. Random synaptic feedback weights support error backpropagation for deep learning. *Nature Communications* **7**, 13276 (2016).
- [10] Nokland, A. Direct feedback alignment provides learning in deep neural networks. In *Proceedings of the 30th International Conference on Neural Information Processing Systems*, NIPS’16, 1045–1053 (Curran Associates Inc., Red Hook, NY, USA, 2016).
- [11] Richards, B. *et al.* A deep learning framework for neuroscience. *Nature Neuroscience* **22**, 1761–1770 (2019).
- [12] Bailey, C., Giustetto, M., Huang, Y.-Y., Hawkins, R. & Kandel, E. Is heterosynaptic modulation essential for stabilizing hebbian plasticity and memory? *Nature reviews. Neuroscience* **1**, 11–20 (2000).
- [13] Turrigiano, G., Leslie, K., Desai, N., Rutherford, L. & Nelson, S. Activity-dependent scaling of quantal amplitude in neocortical neurons. *Nature* **391**, 892–6 (1998).
- [14] Ghosh-Dastidar, S. & Adeli, H. Spiking neural networks. *International Journal of Neural Systems* **19**, 295–308 (2009).
- [15] Sinz, F. H., Pitkow, X., Reimer, J., Bethge, M. & Tolias, A. S. Engineering a less artificial intelligence. *Neuron* **103**, 967–979 (2019).
- [16] Chicca, E. & Indiveri, G. A recipe for creating ideal hybrid memristive-CMOS neuromorphic processing systems. *Applied Physics Letters* **116**, 120501 (2020).
- [17] Williams, S. R. & Stuart, G. J. *Synaptic Integration* (American Cancer Society, 2001).
- [18] Etherington, S. J., Atkinson, S. E., Stuart, G. J. & Williams, S. R. Synaptic integration. *Encyclopedia of Life Sciences* (2010).
- [19] Williams, S. & Atkinson, S. Dendritic synaptic integration in central neurons. *Current biology : CB* **18**, R1045–7 (2008).
- [20] Li, X., Luo, S. & Xue, F. Effects of synaptic integration on the dynamics and computational performance of spiking neural network. *Cognitive Neurodynamics* **14**, 347–357 (2020).
- [21] Royer, S. & Paré, D. Conservation of total synaptic weight through balanced synaptic depression and potentiation. *Nature* **422**, 518–22 (2003).
- [22] Fiete, I. R., Senn, W., Wang, C. Z. H. & Hahnloser, R. H. R. Spike-time-dependent plasticity and heterosynaptic competition organize networks to produce long scale-free sequences of neural activity. *Neuron* **65**, 563–576 (2010).
- [23] Turrigiano, G. The self-tuning neuron: Synaptic scaling of excitatory synapses. *Cell* **135**, 422–35 (2008).
- [24] Moulin, T. C., Rayée, D., Williams, M. J. & Schiöth, H. B. The synaptic scaling literature: A systematic review of methodologies and quality of reporting. *Frontiers in Cellular Neuroscience* **14**, 164 (2020).

- [25] Iбата, K., Sun, Q. & Turrigiano, G. Rapid synaptic scaling induced by changes in postsynaptic firing. *Neuron* **57**, 819–26 (2008).
- [26] Nøkland, A. & Eidnes, L. H. Training neural networks with local error signals. In *Proceedings of the 36th International Conference on Machine Learning*, vol. 97, 4839–4850 (2019).
- [27] Bengio, Y., Lee, D.-H., Bornschein, J., Mesnard, T. & Lin, Z. Towards biologically plausible deep learning (2016). Preprint at <https://arxiv.org/abs/1502.04156>.
- [28] Abraham, W. Metaplasticity: Tuning synapses and networks for plasticity. *Nature reviews. Neuroscience* **9**, 387 (2008).
- [29] Pfeiffer, M., Nessler, B., Douglas, R. J. & Maass, W. Reward-Modulated Hebbian Learning of Decision Making. *Neural Computation* **22**, 1399–1444 (2010).
- [30] Legenstein, R., Chase, S. M., Schwartz, A. B. & Maass, W. A reward-modulated hebbian learning rule can explain experimentally observed network reorganization in a brain control task. *Journal of Neuroscience* **30**, 8400–8410 (2010).
- [31] Frémaux, N., Sprekeler, H. & Gerstner, W. Functional requirements for reward-modulated spike-timing-dependent plasticity. *Journal of Neuroscience* **30**, 13326–13337 (2010).
- [32] Soltoggio, A. & Stanley, K. O. From modulated hebbian plasticity to simple behavior learning through noise and weight saturation. *Neural Networks* **34**, 28–41 (2012).
- [33] Spruston, N. Pyramidal neurons: dendritic structure and synaptic integration. *Nature reviews. Neuroscience* **9**, 206–21 (2008).
- [34] Nesterov, Y. A method for solving the convex programming problem with convergence rate $o(1/k^2)$. *Proceedings of the USSR Academy of Sciences* **269**, 543–547 (1983).
- [35] Tieleman, T. & Hinton, G. Lecture 6.5—RmsProp: Divide the gradient by a running average of its recent magnitude. COURSERA: Neural Networks for Machine Learning (2012).
- [36] Darken, C., Chang, J. & Moody, J. Learning rate schedules for faster stochastic gradient search. In *Neural Networks for Signal Processing II Proceedings of the 1992 IEEE Workshop*, 3–12 (1992).
- [37] LeCun, Y. & Cortes, C. MNIST handwritten digit database (2010). URL <http://yann.lecun.com/exdb/mnist/>.
- [38] Michaelis, L. & Menten, M. Kinetik der invertinwirkung. *Biochem. Zeitung* **49**, 333–369 (1913).
- [39] Cireşan, D. C., Meier, U., Gambardella, L. M. & Schmidhuber, J. Deep, big, simple neural nets for handwritten digit recognition. *Neural Computation* **22**, 3207–3220 (2010).
- [40] Xiao, H., Rasul, K. & Vollgraf, R. Fashion-MNIST: a Novel Image Dataset for Benchmarking Machine Learning Algorithms (2017). Preprint at <https://arxiv.org/abs/1708.07747>.
- [41] Cohen, G., Afshar, S., Tapson, J. & van Schaik, A. Emnist: Extending mnist to handwritten letters. In *2017 International Joint Conference on Neural Networks (IJCNN)*, 2921–2926 (2017).
- [42] Krizhevsky, A., Nair, V. & Hinton, G. Cifar-10 (canadian institute for advanced research) URL <http://www.cs.toronto.edu/~kriz/cifar.html>.
- [43] Bartunov, S. *et al.* Assessing the scalability of biologically-motivated deep learning algorithms and architectures. In *Proceedings of the 32nd International Conference on Neural Information Processing Systems, NIPS’18*, 9390–9400 (2018).
- [44] Frenkel, C., Lefebvre, M. & Bol, D. Learning without feedback: Direct random target projection as a feedback-alignment algorithm with layerwise feedforward training (2019). Preprint at <https://arxiv.org/abs/1909.01311>.
- [45] Muñoz-Martín, I. *et al.* Unsupervised learning to overcome catastrophic forgetting in neural networks. *IEEE Journal on Exploratory Solid-State Computational Devices and Circuits* **5**, 58–66 (2019).
- [46] Kemker, R., McClure, M., Abitino, A., Hayes, T. & Kanan, C. Measuring catastrophic forgetting in neural networks. *Proceedings of the AAAI Conference on Artificial Intelligence* **32** (2018).
- [47] Kirkpatrick, J. *et al.* Overcoming catastrophic forgetting in neural networks. *Proceedings of the National Academy of Sciences* **114**, 3521–3526 (2017).
- [48] Sodhani, S., Chandar, S. & Bengio, Y. Toward training recurrent neural networks for lifelong learning. *Neural Computation* **32**, 1–35 (2020).
- [49] Carrillo, S. *et al.* Scalable hierarchical network-on-chip architecture for spiking neural network hardware implementations. *IEEE Transactions on Parallel and Distributed Systems* **24**, 2451–2461 (2013).
- [50] Pfeiffer, M. & Pfeil, T. Deep learning with spiking neurons: Opportunities and challenges. *Frontiers in Neuroscience* **12**, 774 (2018).
- [51] Wozniak, S., Pantazi, A., Bohnstingl, T. & Eleftheriou, E. Deep learning incorporating biologically inspired neural dynamics and in-memory computing. *Nature Machine Intelligence* **2**, 325–336 (2020).
- [52] Gerstner, W., Kistler, W. M., Naud, R. & Paninski, L. *Neuronal Dynamics: From Single Neurons to Networks and Models of Cognition. Introduction: neurons and mathematics*, 3–27 (Cambridge University Press, 2014).
- [53] Pehlevan, C. & Chklovskii, D. B. Neuroscience-inspired online unsupervised learning algorithms: Artificial neural networks. *IEEE Signal Processing Magazine* **36**, 88–96 (2019).
- [54] Chistiakova, M., Bannon, N. M., Bazhenov, M. & Volgushev, M. Heterosynaptic plasticity: Multiple mechanisms and multiple roles. *The Neuroscientist* **20**, 483–498 (2014).
- [55] Caya-Bissonnette, L. Heterosynaptic plasticity in cortical interneurons. *Journal of Neuroscience* **40**, 1793–1794 (2020).
- [56] Buzsáki, G. & Mizuseki, K. The log-dynamic brain: How skewed distributions affect network operations. *Nature reviews. Neuroscience* **15**, 264–278 (2014).
- [57] Iyer, R., Menon, V., Buice, M., Koch, C. & Mihalas, S. The influence of synaptic weight distribution on neuronal population dynamics. *PLOS Computational Biology* **9**, 1–16 (2013).
- [58] Teramae, J. & Fukai, T. Computational implications of lognormally distributed synaptic weights. *Proceedings of the IEEE* **102**, 500–512 (2014).
- [59] Song, S., Sjöström, P. J., Reigl, M., Nelson, S. & Chklovskii, D. B. Highly nonrandom features of synaptic connectivity in local cortical circuits. *PLOS Biology* **3**, e68 (2005).
- [60] He, K., Zhang, X., Ren, S. & Sun, J. Delving deep into rectifiers: Surpassing human-level performance on ima-

- genet classification. In *Proceedings of the IEEE International Conference on Computer Vision (ICCV)*, 1026–1034 (2015).
- [61] Glorot, X. & Bengio, Y. Understanding the difficulty of training deep feedforward neural networks. In *Proceedings of the Thirteenth International Conference on Artificial Intelligence and Statistics*, vol. 9, 249–256 (2010).
- [62] Hinton, G. E., Srivastava, N., Krizhevsky, A., Sutskever, I. & Salakhutdinov, R. Improving neural networks by preventing co-adaptation of feature detectors (2012). Preprint at <https://arxiv.org/abs/1207.0580>.